


# The Process of Engraftment of Myogenic Cells in Skeletal Muscles of Primates: Understanding Clinical Observations and Setting Directions in Cell Transplantation Research

Cell Transplantation  
2017, Vol. 26(11) 1763–1779  
© The Author(s) 2017  
Reprints and permission:  
sagepub.com/journalsPermissions.nav  
DOI: 10.1177/0963689717724798  
journals.sagepub.com/home/cll  


Daniel Skuk<sup>1</sup> and Jacques P. Tremblay<sup>1</sup>

## Abstract

We studied in macaques the evolution of the intramuscular transplantation of muscle precursor cells between the time of administration and the time at which the graft is considered stable. Satellite cell–derived myoblasts labeled with  $\beta$ -galactosidase were transplanted into 1 cm<sup>3</sup> muscle regions following cell culture and transplantation protocols similar to our last clinical trials. These regions were biopsied 1 h, 1, 3, 7 d, and 3 wk later and analyzed by histology. We observed that the cell suspension leaks from the muscle bundles during injection toward the epimysium and perimysium, where most cells accumulate after transplantation. We observed evidence of necrosis, apoptosis, and mitosis in the accumulations of grafted cells, and of potential migration to participate in myofiber regeneration in the surrounding muscle bundles. After 3 wk, the compact accumulations of grafted cells left only some graft-derived myotubes and small myofibers in the perimysium. Hybrid myofibers were abundant in the muscle fascicles at 3 wk posttransplantation, and they most likely occur by grafted myoblasts that migrated from the peripheral accumulations than by the few remaining within the fascicles immediately after injection. These observations explain the findings in clinical trials of myoblast transplantation and provide information for the future research in cell therapy in myology.

## Keywords

cell distribution, cell migration, intramuscular cell transplantation, myofiber, satellite cell–derived myoblast, skeletal muscle

## Introduction

Intramuscular transplantation of muscle-precursor cells (MPCs), that is, mononuclear cells that are precursors of myofibers, has potential applications for the treatment of skeletal muscle pathologies. Its therapeutic effect may be due to 2 properties<sup>1</sup>:

- (a) Grafted MPCs can be recruited by the myofibers already present in the muscle in order to fuse with them. These myofibers will then contain graft-derived myonuclei that may allow genetic complementation, thus producing graft-derived proteins with a therapeutic effect (e.g., proteins whose absence cause myofiber pathology).
- (b) On the other hand, grafted MPCs can fuse with each other to form graft-derived myotubes, which under appropriate conditions such as innervation,<sup>2</sup> could differentiate in myofibers. This property should be useful for regenerative medicine approaches,

searching to restore a functional structure in muscles that were decimated by a degenerative myopathy or lost myofibers by other causes.

Among the diverse mononuclear cells that have been transplanted in animal models seeking for these properties,<sup>1,3</sup> the most widely used were satellite cell–derived myoblasts (SCDMs, “satellite cell derived” is specified to avoid confusion between myoblasts involved in postnatal myofiber

<sup>1</sup> Axe Neurosciences, Research Center of the CHU de Québec–CHUL, Québec, Canada

Submitted: April 20, 2017. Revised: July 11, 2017. Accepted: July 12, 2017.

### Corresponding Author:

Daniel Skuk, Axe Neurosciences, Research Center of the CHU de Québec–CHUL, P-09300, CHUL, 2705 boulevard Laurier, Québec, QC, Canada G1V 4G2.

Email: daniel.skuk@crchudequebec.ulaval.ca



**Table 1.** Monkeys Included in the Study, Indicating Details of the Protocol.

Monkey Number	Species	Weight (Kg)	Days of Cell		Amount of Cells Per Site	Density of Injections	Volume per Injection	Tacrolimus	Timing of Biopsies Post-CT
			Culture After Thawing	Cell Viability <sup>a</sup> (%)					
1	Cynomolgus	7.5	11	92	$12 \times 10^6$	25/cm <sup>2</sup>	10 $\mu$ L	—	1 h, 1 d, 3 d, 7 d
2	Cynomolgus	7.9	11	92	$12 \times 10^6$	25/cm <sup>2</sup>	10 $\mu$ L	—	1 h, 1 d, 3 d, 7 d
3	Cynomolgus	5.6	13	92	$8.5 \times 10^6$	100/cm <sup>2</sup>	5 $\mu$ L	—	1 h, 1 d, 3 d, 7 d
4	Cynomolgus	7	7	99	$18.8 \times 10^6$	100/cm <sup>2</sup>	5 $\mu$ L	—	1 h, 1 d, 3 d, 7 d
5	Rhesus	7	6	90.5	$5.4 \times 10^6$	100/cm <sup>2</sup>	5 $\mu$ L	Yes	1 h, 1 d, 3 d, 7 d, 3 wk
6	Cynomolgus	4.9	11	94	$8.6 \times 10^6$	100/cm <sup>2</sup>	5 $\mu$ L	Yes	1 h, 1 d, 3 d, 7 d, 3 wk
7	Cynomolgus	3.9	7	95.5	$13.1 \times 10^6$	100/cm <sup>2</sup>	5 $\mu$ L	Yes	1 h, 1 d, 3 d, 7 d, 3wk

Abbreviations: d, day; h, hour; wk, week.

<sup>a</sup>A trypan blue exclusion test.

regeneration, that is, SCDMs, and somite-derived myoblasts involved in muscle embryogenesis). In clinical transplantation, SCDMs definitely produced the first outcome,<sup>4-9</sup> and there is histological evidence that they produced the second one.<sup>10</sup> In fact, the ectopic presence of myofibers in a human heart injected with SCDMs is clinical evidence that grafted SCDMs can form new myofibers in humans.<sup>11</sup>

The first clinical objective of SCDM transplantation was to restore dystrophin in muscles of patients with Duchenne muscular dystrophy (DMD).<sup>12</sup> Subsequently, other clinical applications sought to improve individual muscles affected by more local processes, such as the cricopharyngeal muscle in oculopharyngeal muscular dystrophy,<sup>13</sup> the tibialis anterior in fascioscapular muscular dystrophy,<sup>14</sup> the urinary sphincter in stress urinary incontinence,<sup>15</sup> and the external anal sphincter in anal incontinence.<sup>16</sup>

Indeed, appropriate protocols of cell transplantation (CT) should be based on clear comprehension of how the grafted cells interact with the host tissue. If this aspect is speculated rather than endorsed by observation, there is the risk of using incorrect CT protocols, thus missing the possibility of reaching clinical results. In fact, one of the obscure points in this topic is surprisingly basic: we do not know exactly how the grafted MPCs interact with the host tissue in a healthy or diseased muscle to generate the graft outcomes mentioned above.

The best models for human extrapolation in preclinical transplantation research are nonhuman primates, among which the most commonly used species are those of the genus *Macaca*.<sup>17</sup> Since both are primates of the parvorder *Catarrhini*, macaques and humans share optimal similarities in transplantation biology.<sup>17</sup> Otherwise, the muscle structure and size in macaques are more appropriate to test CT protocols, and the production of SCDMs for transplantation (cell isolation, media and supplements, and final cell population) is identical to humans.<sup>18</sup> Indeed, the research in macaques allowed to be more predictive than before in clinical trials of SCDM transplantation.<sup>19</sup>

Continuing this line of research, this study provides a first analysis of the natural course of the intramuscular graft of MPCs in healthy muscles of primates, between the time the cells are administered and the moment at which the graft can be considered stable, that is, when the processes of cell fusion and myofiber regeneration are finished, using a CT protocol similar to our last clinical trials.<sup>5,6,8,9</sup>

## Materials and Methods

### Animals

We included 7 male macaques (6 cynomolgus, *Macaca fascicularis*, weight 3.9 to 7.9 kg; and 1 rhesus, *Macaca mulatta*, 4 years old) as recipients of allogeneic SCDM transplantation (Table 1). For CT and biopsies, monkeys were kept under general anesthesia using isoflurane (1.5% to 2% in oxygen; Abbott Laboratories, Montreal, Québec, Canada) after induction with ketamine (IM, 10 mg/kg; Bioniche, Belleville, Ontario, Canada) and glycopyrrolate (IM, 0.05 mg/kg; Sandoz Canada, Boucherville, Québec, Canada). Buprenorphine (0.01 mg/kg twice daily for 3 d; Champion Alstoe, Whitby, Ontario, Canada) was given intramuscularly for postoperative analgesia.

### Cell Culture

SCDMs were obtained from muscle biopsies performed in a gastrocnemius in cynomolgus and rhesus monkeys. The muscle biopsies were minced with fine scissors into fragments of less than 1 mm<sup>3</sup> and then dissociated with 0.2% collagenase (Sigma, St Louis, MO, USA) in Hank's balanced salt solution (HBSS; Gibco, Grand Island, NY, USA) for 1 h, followed by another dissociation in 0.125% trypsin (Gibco) in HBSS for 45 min. The isolated cells were subcultured in vitro in MCDB (Molecular, Cellular, and Developmental Biology) 120 culture medium<sup>20</sup> with 15% fetal bovine serum (FBS, Hyclone, Logan, UT, USA), 10 ng/mL basic fibroblast growth factor (Feldan, St-Laurent, Québec, Canada), 0.5 mg/mL bovine serum albumin (BSA)

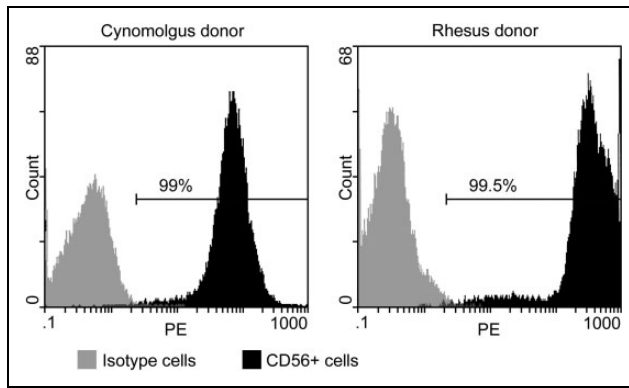


**Figure 1.** Flow cytometry results in the cultured cells to determine the percentage of CD56<sup>+</sup> cells (used as an indicator of the percentage of satellite cell-derived myoblast [SCDMs]).

(Sigma), 1.0  $\mu$ M dexamethasone (Sigma), and 5  $\mu$ g/mL human insulin (Sigma). The cells were infected in vitro with a replication-defective retroviral vector LNPoZC7 (gift of Dr Constance Cepko, Harvard University, Boston, MA, USA) encoding a lacZ reporter gene and a neomycin-resistance gene. This was done twice with the first subculture. The transduced cells were selected twice with 600  $\mu$ g/mL Geneticin<sup>®</sup> (Invitrogen, Burlington, Ontario, Canada) within 4 d, proliferated until confluence, and frozen for storage in liquid nitrogen. A sample of cells to be frozen was analyzed to determine the percentage of CD56<sup>+</sup> cells as an indicator of the percentage of SCDMs. These cells were incubated with a phycoerythrin-coupled anti-CD56 antibody (Beckman Coulter, Fullerton, CA, USA) and analyzed in a Coulter Epics XL flow cytometer (Beckman Coulter). In all, 99% of the cells of cynomolgus donor and 99.5% of the cells of rhesus donor, respectively, were CD56<sup>+</sup> (Fig. 1).

### Cell Transplantation

For transplantation, frozen cells were thawed and proliferated in 75-cm<sup>2</sup> flasks. All cells were transplanted after the second subculture (passage 2). Then, the cells were detached from the flasks using 0.1% trypsin in HBSS and washed 3 times with HBSS. The final cell pellets were resuspended in HBSS and injected as indicated below. A sample of cells was used to verify the cell viability with a trypan blue exclusion method (Table 1). For this, we added 0.1 mL of a 0.4% trypan blue (Sigma) solution to 1 mL of the cell suspension that was loaded in a hemocytometer and examined under an inverted microscope (Bausch & Lomb Place, Rochester, NY, USA).

Intramuscular cell injections were performed percutaneously, using matrices of parallel equidistant injections.<sup>21</sup> CT was performed either with 50  $\mu$ L precision syringes alone (Hamilton, Reno, NV, USA) or with 250  $\mu$ L precision syringes (Hamilton) attached to a PB600-1 repeating dispenser (Hamilton) using 27-gauge 0.5-inch disposable needles

(Terumo, Somerset, NJ, USA). Matrices of injections were performed at 2 densities of injections: 25 per cm<sup>2</sup> and 100 per cm<sup>2</sup>, in about 1 cm<sup>3</sup> of muscle, as in our previous clinical trial.<sup>5</sup> Each injection was perpendicular to the surface of the muscle, penetrating to the maximum depth of the needle, and the cell suspension (5 or 10  $\mu$ L per injection) was delivered in the needle trajectory uniformly during the needle withdrawal. OpSite sterile transparent dressings with a 5-mm grid (Smith & Nephew, Hull, United Kingdom) were adhered to the skin to control the pattern and density of injections. The amount of cells injected varied with the quantity obtained at the moment of transplantation (Table 1). To identify the injected muscle sites for later biopsies, stitches of inert nonabsorbable polypropylene 4.0 suture (Prolene, Ethicon Inc., Somerville, NJ, USA) were placed roughly 5 mm on both sides of each transplantation site. The muscles used for CT were the *biceps brachii*, *quadriceps femoris*, and *gastrocnemius*.

### Immunosuppression

Monkeys #5 to #7, which were analyzed over a longer period than the others (i.e., 3 wk post-CT), were immunosuppressed using an intramuscular formulation of tacrolimus (a generous gift from Astellas Pharma Inc., Osaka, Japan), beginning 5 to 7 d before transplantation and maintained until the end of the experiment. Tacrolimus was injected intramuscularly once a day, beginning at 0.5 mg/kg/d and adjusting the dosage to target the blood levels of more than 50  $\mu$ g/L, as quantified in blood samples with an IMx tacrolimus II kit for micro-particle enzyme immunoassay (Abbott, Wiesbaden, Germany).

### Sampling

Biopsies were performed in the CT sites at 1 h, 1, 3, and 7 d in all monkeys, and at 3 wk in monkeys #5 to #7. To choose these periods, we rely on previous observations about post-CT myofiber regeneration in mice and monkeys.<sup>22–25</sup> Thus, 1 h was chosen to see the immediate distribution of the grafted cells after saline absorption, 1 d to see earlier changes, 3 d to target the peak of macrophage myofiber invasion, 7 d to target ongoing myofiber regeneration, and 3 wk to observe the muscle after regeneration has been completed. Biopsies were mounted in embedding medium, snap-frozen in liquid nitrogen, and stored at  $-80^{\circ}$ C until performing serial sections of 10 to 15  $\mu$ m in a cryostat at  $-25^{\circ}$ C.

### Histological Analysis

Sections of each biopsy were stained with hematoxylin and eosin (H&E) to analyze the general structure of the muscle and mounted in synthetic resin. To detect damaged myofibers in the early periods, sections were stained for 5 min in a 2% alizarin red (Sigma, Oakville, Canada) solution at pH

5.4, followed by a brief rinse in water at pH 5.4, then in acetone, acetone/toluene 1:1, and toluene, to be mounted in synthetic resin. For  $\beta$ -galactosidase ( $\beta$ -Gal) histochemical detection, muscle sections were fixed for 3 min in 0.25% glutaraldehyde, rinsed with phosphate-buffered saline (PBS), incubated for 24 h at room temperature in a solution of 0.4 mg/mL X-gal (5-bromo-4-chloro-3-indolyl- $\beta$ -D-galactopyranoside; Boehringer Mannheim, Vienna, Austria) containing 1 mM  $MgCl_2$ , 3 mM  $Ke_3F(CN)_6$ , 3 mM  $Ke_4F(CN)_6 \cdot 3H_2O$  in PBS, and mounted in 1:1 glycerin jelly.

Fluorescent immunodetection was performed in the following cases. Desmin was detected using a mouse antidesmin monoclonal antibody (mAb; Dako, Copenhagen, Denmark). The active form of caspase 3<sup>26</sup> was detected with a rabbit antihuman/mouse caspase 3 active polyclonal antibody (R&D Systems, Minneapolis, MN, USA). Complement's membrane attack complex (MAC) was detected using a mouse antihuman/baboon C5b-9 mAb (Abcam, Cambridge, MA, USA). Macrophages were detected with a mouse antihuman CD163 mAb (BD Biosciences, Mississauga, Canada). Proliferating cells were evidenced with a mouse antiproliferating cell nuclear antigen (PCNA) mAb (Sigma). To depict acute rejection,<sup>27</sup> we detected CD8+ lymphocytes using a mouse antihuman/maaque CD8 mAb (BD Biosciences). For immunodetection techniques, non-specific binding was blocked by a 30 min incubation with 10% FBS in PBS. Sections were incubated 1 h with the primary antibody at the concentrations recommended by the manufacturers. This was followed by a 30-min incubation with a biotinylated antimouse antibody (1/150, Dako) or a biotinylated antirabbit antibody (1/150, Dako) followed by a 30-min incubation with streptavidin-Cy3 (1/700, Sigma). For double immunostaining, an antimouse immunoglobulin G (IgG) antibody conjugated to Alexa Fluor 488 (1:300; Molecular Probes, Eugene, OR, USA) was also used as second antibody. Antibodies and streptavidin were diluted in PBS, pH 7.4, containing 1% FBS. Incubations were performed at room temperature. Sections of tissues from macaques were used as positive controls. The reactivity of the primary antibodies used in this study with macaque proteins had been previously tested.

The muscle sections were analyzed using an Axiophot microscope with epifluorescence and bright field optics (Zeiss, Oberkochen, Germany). Pictures were taken with an A650 IS digital camera (Canon, Tokyo, Japan).

### Quantitative Analysis

To estimate the amount of  $\beta$ -Gal in some biopsies, we measured in digital images the area occupied by  $\beta$ -Gal in the sections containing more  $\beta$ -Gal, as well as the total area of the respective biopsy cross section, using NIH ImageJ 1.49v software, and then we calculated the percentage of the section occupied by  $\beta$ -Gal. For the bar graph, we estimated the mean value of  $n = 3$  monkeys  $\pm 1$  standard deviation. An analysis of variance test with post hoc tests was used to

assess the probability of significant differences between post-CT periods (significance in the figure corresponds to the Tukey and Bonferroni results). Statistical significance was defined as  $P < 0.05$ .

### Revision of Previous Results of SCDM Transplantation in Humans

To complete this study, we reviewed the histological material of our previous clinical trials of SCDM allotransplantations in DMD patients.<sup>5,6,8</sup> These clinical studies used a CT technique by matrices of high-density injections similar to that detailed above.<sup>5</sup> In these cases, the cell-grafted muscle regions were evaluated histologically in slides stained with H&E and by immunodetection of the donor-derived dystrophin with monoclonal antibodies specific to epitopes that were present in the cell donor but not in the patient that received the cells (see references<sup>5,6,8,9</sup> for details).

### Results

To describe the cell graft evolution, we will follow a chronological criterion in which each period is analyzed consecutively. During this evolution, 2 main elements modified the normal muscle structure and determined the graft result: (a) the damage caused by the transplantation and (b) the presence of the grafted cells.

#### One Hour Post-CT

In H&E-stained sections, the muscle damage was evident in the form of eosinophilic myofibers, some of them with pale cores or gaps, in regions with focal edema (Fig. 2 A and D). The best technique to evidence damaged myofibers in this period was alizarin red, which stained them in dark red-orange (Fig. 2B). The distribution of the damaged myofibers in the muscle sections reproduced the intramuscular courses of the injection needle (Fig. 2A to C, blue arrows), that is, they formed irregular bands roughly parallel to each other and oriented from the surface to the depth of the biopsy.

The presence of compact collections of mononuclear cells was the other prominent change in the muscle (Fig. 2A and D). These compact collections of cells were of elongated cross sections, very variable sizes, and were mainly in the periphery of muscle bundles. They either dissected the boundary between the muscle bundles and the perimysium or cleaved the perimysium in several fragmented layers (Fig. 2D).  $\beta$ -Gal detection (Fig. 2C) showed that these cell accumulations were  $\beta$ -Gal+ and, therefore, confirmed that they were the grafted cells. Most  $\beta$ -Gal was observed in the perimysial accumulations of cells, which were either more or less distributed across the biopsy or eccentrically located at the deepest part of the biopsy. Few  $\beta$ -Gal+ elements were observed in the intrafascicular trajectories of damaged myofibers (Fig. 2C).

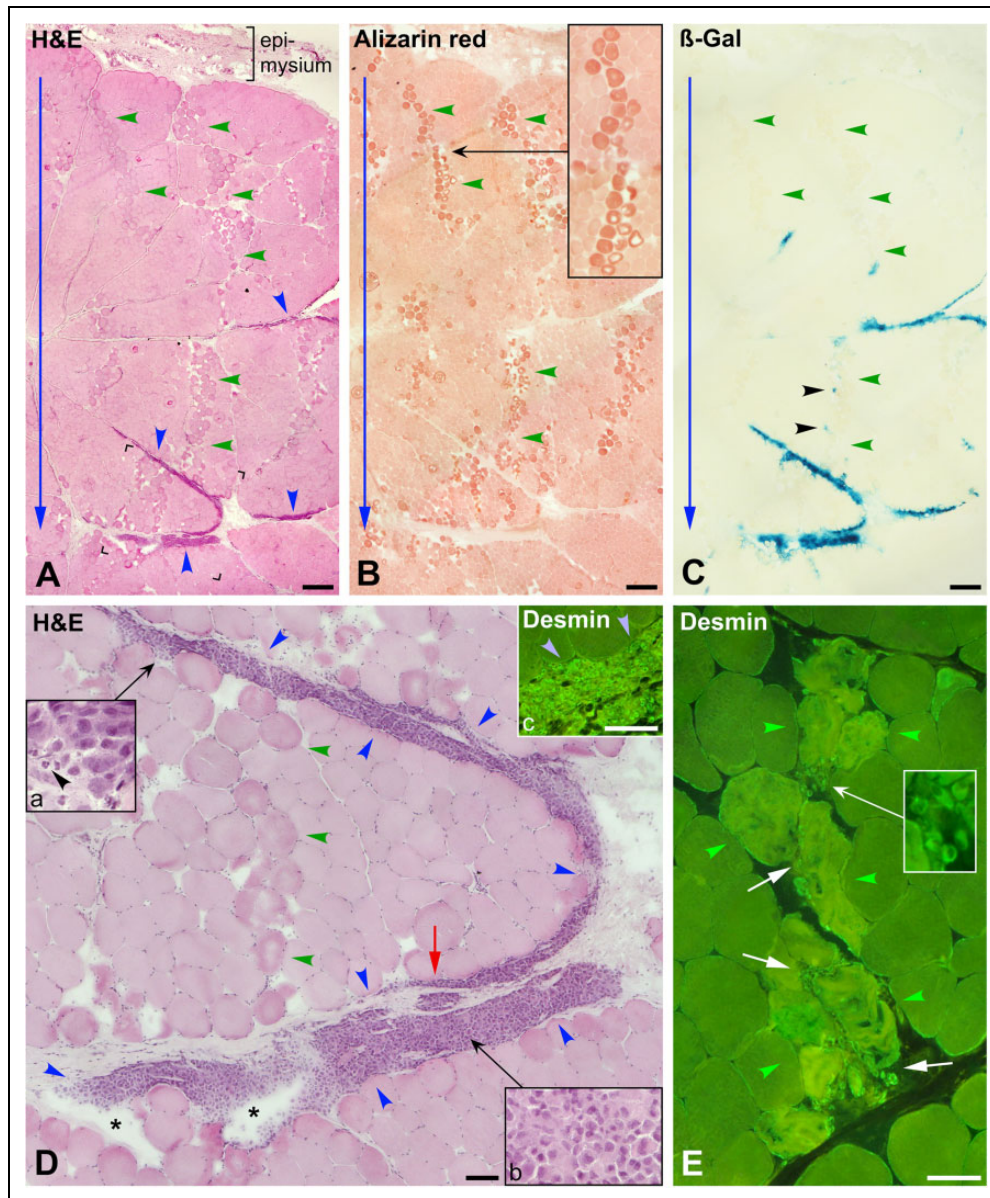


**Figure 2.** Muscle biopsies 1 h post-cell transplantation (CT). (A) to (C) are serial sections stained with hematoxylin and eosin (H&E), alizarin red, and for  $\beta$ -Gal detection (monkey #4, biceps brachium). The outer muscle surface is upward, and blue arrows indicate the direction of the needle penetrations. (A) Myofibers damaged by the injections are darker, sometimes with a pale core or disrupted sarcoplasm, and form irregular bands (some indicated with green arrowheads) in which there is some edema. The dark red-orange coloration of alizarin red further evidences damaged myofibers (B, the inset highlights a linear distribution of damaged myofibers).  $\beta$ -Gal (C, dark greenish blue) evidences the grafted cells, which mostly correspond to accumulations of mononuclear cells in A (blue arrowheads). There is no  $\beta$ -Gal in most of the injection trajectories, with the exception of some elements indicated with black arrowheads (C). Histological details are more clearly seen in D, an enlargement of the region between corners in (A). The accumulation of grafted cells (between blue arrowheads) split the boundary between the muscle bundle and the epimysium and also split the perimysium in layers (red arrow). Asterisks indicate edema or nonabsorbed saline in the accumulation of grafted cells. Green arrowheads point a band of damaged myofibers with edema corresponding to an injection trajectory. Insets “a” and “b” show that the accumulation of grafted cells is quite homogeneous, with the exception of a few polymorphonuclear leucocytes (black arrowhead). Inset “c” shows by desmin immunodetection that these accumulations of grafted cells (blue arrowheads) are essentially desmin+. (E) Desmin immunodetection (monkey #2, biceps brachium). Myofibers damaged by an injection (between green arrowheads) have increased staining and “ragged” appearance. Some desmin+ mononuclear cells (white arrows and inset) are between these damaged myofibers. Scale bars = 500  $\mu$ m (A to C) and 100  $\mu$ m (D and E).

Desmin immunodetection confirmed that the cell collections were essentially desmin+, as expected for grafted SCDMs. Few desmin+ mononuclear cells were observed

in some intrafascicular needle trajectories between the damaged myofibers (Fig. 1E). Since 1 h after myofiber damage is too early to observe proliferation of endogenous SCDMs,

these desmin+ mononuclear cells should correspond to the injected SCDMs. Similar extrapolation was not possible in later periods because of the later proliferation of endogenous SCDMs.

### Day 1 Post-CT

The edema in the muscle bundles was reabsorbed, and the damaged/necrotic myofibers were identified in H&E-stained sections by the disappearance of the intermyofibrillar network (initial phase of the "hyaline myofibers" in muscle pathology<sup>28</sup>) and the incipient invasion of inflammatory cells (Fig. 3C, F, and I). MAC immunodetection was the best technique to evidence damaged myofibers at this period (Fig. 3E and H). Intracellular MAC staining was clear in damaged myofibers (in contrast to 1 h post-CT), whereas alizarin red was blurred. Damaged myofibers were also in irregular bands reproducing the intramuscular courses of the injection needle.

H&E-stained sections again showed collections of mononuclear cells (Fig. 3A, C, F, and I), which were  $\beta$ -Gal+ (Fig. 3B, D and G). They were mainly in the perimysium (Fig. 3A, B, F, G and I) but also in the outer muscle surface when the epimysium was preserved in the section (Fig. 3A to E).  $\beta$ -Gal was observed in some intrafascicular injection trajectories (Fig. 3G), although this was not frequent and in some cases they were in fact in thinner layers of perimysium. We observed some rarefaction of the grafted-cell collections compared to 1 h post-CT, that is, they were less compact, and the cell staining was weaker, with nuclear fading suggestive of karyolysis (Fig. 3I). There was also a significant infiltration by polymorphonuclear leukocytes (Fig. 3C and I).

### Day 3 Post-CT

Damaged myofibers exhibited partial or complete phagocytosis in this period, so the best techniques for evidencing them were H&E (Fig. 4A, D and G) and immunodetection of macrophages (Fig. 4B, E and H). MAC immunodetection and alizarin red were blurred and limited to some myofibers, which is explained by the phagocytosis of necrotic myofiber debris. Again, myofibers undergoing phagocytosis reproduced the intramuscular courses of the injection needle (Fig. 4A and B). There was some macrophage infiltration in perimysial regions containing  $\beta$ -Gal+ elements, but this was more diffuse and less intense than in the regions of myofiber phagocytosis (Fig. 4F to H).

The predominant accumulations of mononuclear cells in this period were those of phagocytes, and there were no compact accumulations of mononuclear cells in the perimysium, so it was impossible to locate the grafted cells without the aid of  $\beta$ -Gal staining.  $\beta$ -Gal stain was generally fainter than in the previous periods and was more distributed between the perimysium and the intrafascicular bands of damaged myofibers (Fig. 4C and F).

### Day 7 Post-CT

Histological evidence of acute rejection, in the form of dense lymphocyte accumulations with CD8+ cells,<sup>27</sup> was observed in nonimmunosuppressed monkeys. As this interferes with the natural evolution of the graft, the description of this period refers to the immunosuppressed monkeys, in which there was no evidence of rejection.

At this time, there were no damaged/necrotic myofibers but regenerating myofibers, observed with H&E as small basophilic myofibers (Fig. 5C) generally with internal enlarged myonuclei. The distribution of regenerating myofibers reproduced the intramuscular courses of the injection needle (Fig. 5A, C and E). There were no compact accumulations of mononuclear cells.  $\beta$ -Gal expression was slight and essentially in regenerating myofibers (Fig. 5C and D), prefiguring the pattern of bands of engraftment that was visible at later periods (Fig. 6). Some scarce small  $\beta$ -Gal+ elements were observed in the perimysium, some of which were identified as myotubes (Fig. 5C to F).

### 3 Weeks Post-CT

Muscle histology was essentially normal, with the exception of some myofibers with internal nuclei, basophilia and reduced size, and of some angular myofibers, which resulted from some incomplete regeneration in the injection trajectories (Fig. 6D). The vast majority of  $\beta$ -Gal was in intrafascicular myofibers, which were arranged in irregular and roughly parallel bands corresponding to the injection trajectories (Fig. 6B and C), configuring the pattern of bands of engraftment. Monitoring of serial sections confirmed that these were hybrid myofibers, since the expression of  $\beta$ -Gal was in a limited myofiber region. Scarce small  $\beta$ -Gal+ elements were observed in the regions of connective tissue (Fig. 6E and F).

### $\beta$ -Gal Quantification

The distribution of  $\beta$ -Gal through the follow-up showed not only a critical change (from a random location in the perimysium and epimysium to a regular expression in myofibers as bands of engraftment) but also the area of the muscle sections expressing  $\beta$ -Gal seemed to increase significantly at 3 wk. We confirmed that by measuring the area of the biopsy sections occupied by  $\beta$ -Gal in monkeys #5 to #7. As shown in the graph of Fig. 7, the surface occupied by  $\beta$ -Gal in the sections increased from a range of means of 0.8% to 1.8% the first wk post-CT, to an average of 17% at 3 wk post-CT. The changes in the  $\beta$ -Gal distribution, which reflect the behavior of the grafted cells, are illustrated in Fig. 7.

### Cell Death and Proliferation

Since there was a gradual rarefaction of the perimysial accumulations of grafted cells and that this could be at least in part attributable to cell death (also suggested by the images

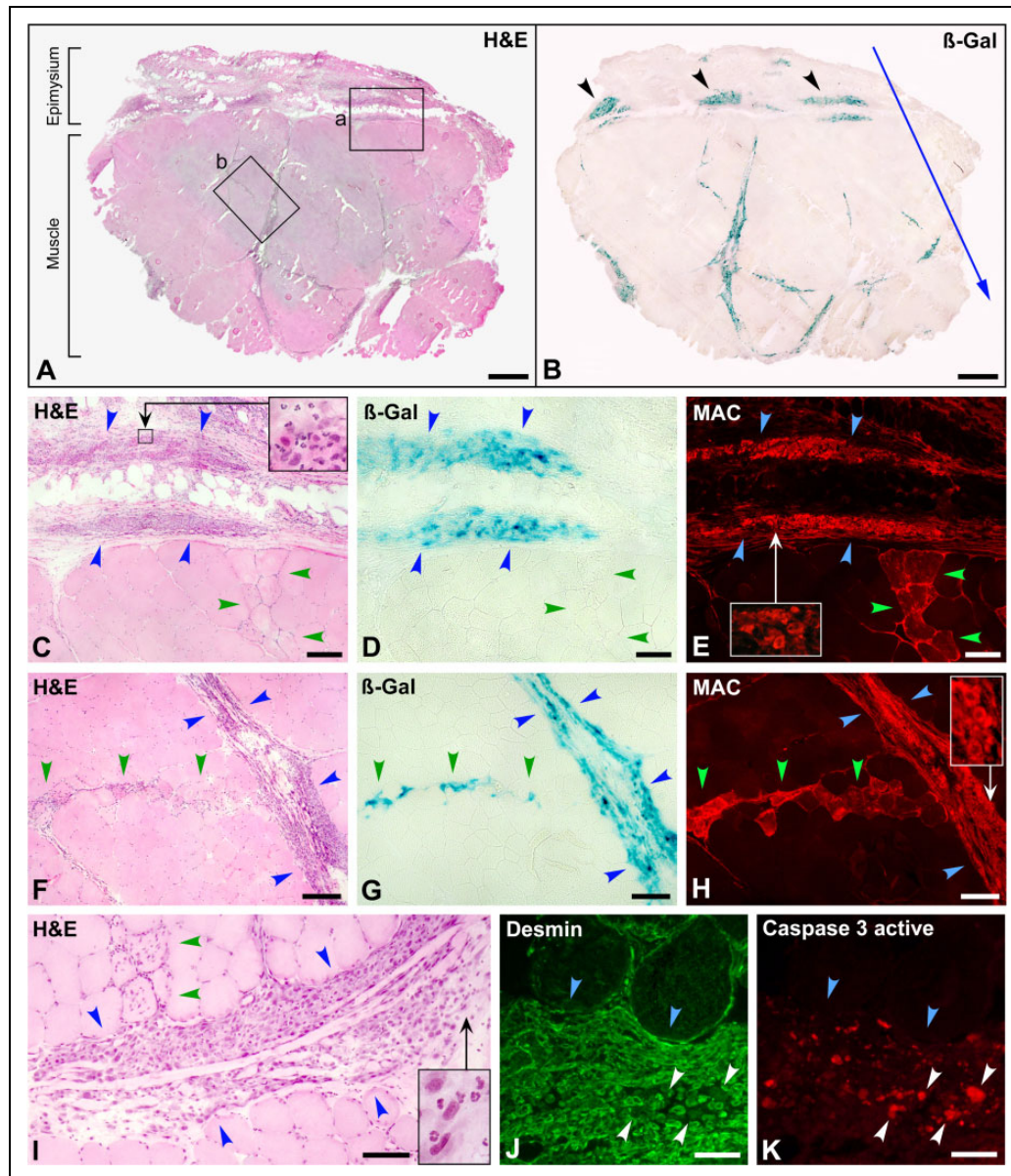


**Figure 3.** Muscle biopsy at post-cell transplantation (CT) day 1 (monkey #1, biceps brachium). (A) and (B) are serial whole cross sections stained with hematoxylin and eosin (H&E) and for  $\beta$ -Gal detection. The outer muscle surface is upward, and the blue arrow indicates the direction of the cell injections. The vast majority of the  $\beta$ -Gal<sup>+</sup> cells are located in the perimysium and epimysium.  $\beta$ -Gal<sup>+</sup> cell accumulations in the epimysium (B, arrowheads) coincide with the points of needle penetration (2 mm from each other) and may represent cell suspension leakage. The region “a” in (A) is enlarged in (C). Blue arrowheads circumscribe an extramuscular cluster of mononuclear cells, and green arrowheads a band of damaged myofibers with incipient infiltration by inflammatory cells, corresponding to the entry of the needle. There are abundant polymorphonuclear leucocytes in these cell clusters (inset).  $\beta$ -Gal staining in a serial section (D) confirms that this cell cluster is of grafted cells. Damaged myofibers are clearly identified in a serial section (E, green arrowheads) by sarcoplasmic membrane attack complex (MAC) detection. Abundant MAC deposition is also detected in the cluster of grafted cells (E, blue arrowheads). The enlargement in the inset evidences cytoplasmic MAC in mononuclear cells. One of the few regions in which  $\beta$ -Gal<sup>+</sup> cells were observed along an injection trajectory (region “b” in A) is enlarged in F, followed by serial sections stained for  $\beta$ -Gal (G) and MAC detection (H). Blue arrowheads circumscribe a perimysial accumulation of grafted cells. A band of myofibers damaged by the injection (green arrowheads) is identified by sarcoplasmic immunodetection of MAC (H). There are  $\beta$ -Gal<sup>+</sup> elements along this band (G). Abundant MAC deposition was also detected in the perimysial accumulation of grafted cells (H) and the enlargement in the inset evidences cytoplasmic MAC in mononuclear cells. (I) shows another perimysial cluster of grafted cells (between blue arrowheads) to show the splitting of the perimysium in several layers. Incipient inflammatory cell infiltration in myofibers damaged by the injection is indicated (green arrowheads). There are also abundant polymorphonuclear cells in the cell accumulation (inset), and nuclear fading suggests karyolysis. Both factors give a more heterogeneous and less compact aspect of the grafted-cell cluster than at 1 h post-CT. Codetection of desmin (J, green fluorescence) and caspase 3 active (K, red fluorescence) shows an intramuscular accumulation of grafted satellite cell-derived myoblasts (SCDMs; blue arrowheads) in which several elements are positive for caspase 3 active (white arrowheads). Scale bars = 1 mm (A, B), 200  $\mu$ m (C to H), 100  $\mu$ m (I), and 50  $\mu$ m (J, K).

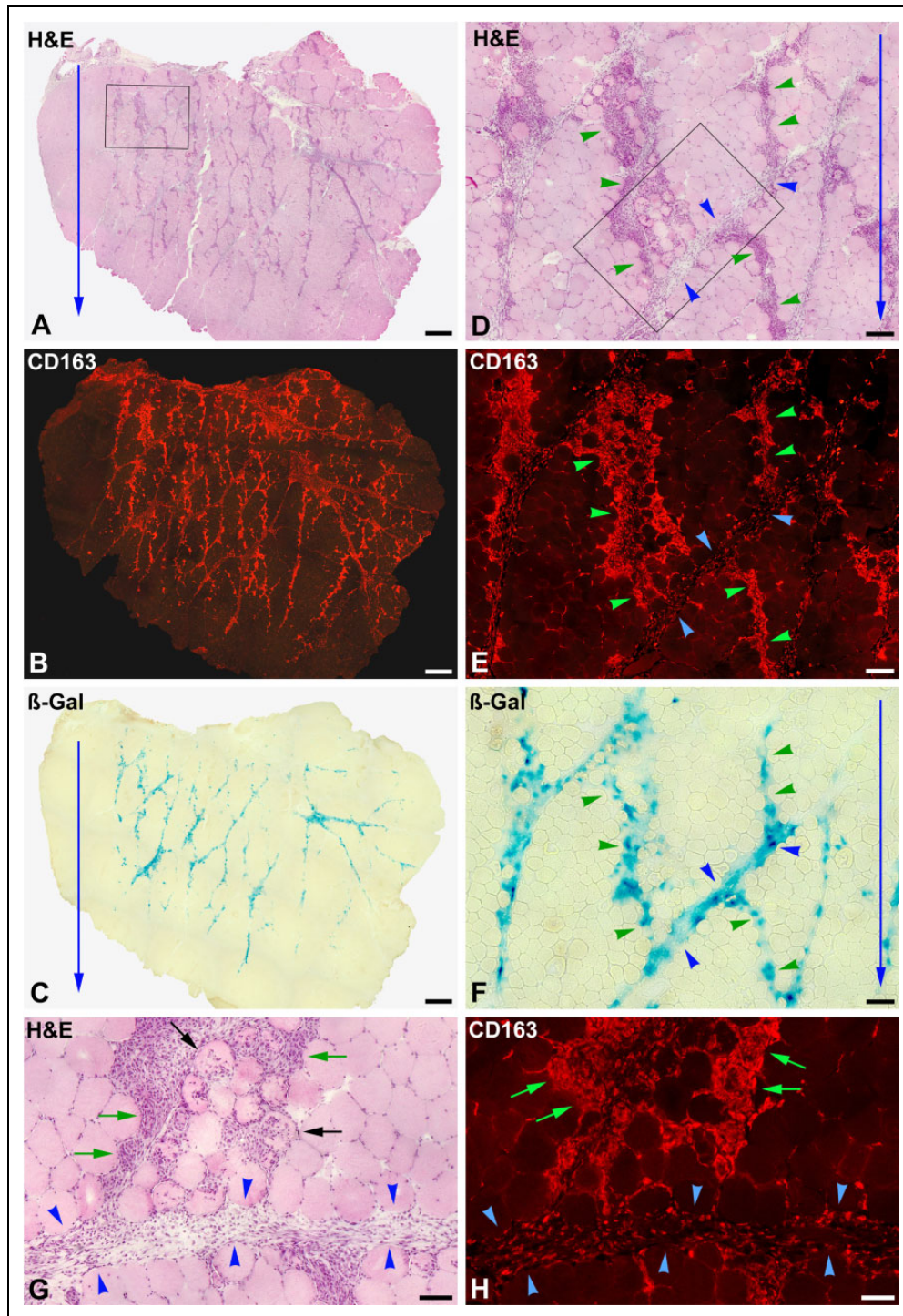


**Figure 4.** Muscle biopsy at post-cell transplantation (CT) day 3 (monkey #4, quadriceps femoris). (A) to (C) are serial whole cross sections. (D) to (F) are enlargements of the rectangle in (A), and (G) and (H) enlargements of the rectangle in (D). Sections were stained with hematoxylin and eosin (H&E) for immunodetection of macrophages (CD163+) and for  $\beta$ -Gal detection. The outer muscle surface is upward, and blue arrows indicate the direction of the cell injections, as evidenced by the roughly parallel basophilic stripes (A), corresponding to myofibers undergoing phagocytosis (D and G), essentially by macrophages (B, E, and H). Macrophage invasion of myofibers is either partial (black arrows) or complete (green arrows). Green arrowheads indicate bands of myofibers undergoing phagocytosis (corresponding to the injection damage), and blue arrowheads indicate regions of perimysium. Macrophage infiltration is dense in the damaged myofibers and more diffuse in the perimysium.  $\beta$ -Gal is quite equally distributed between the perimysium and the bands of damaged myofibers in phagocytosis (C and F). Scale bars = 1 mm (A to C), 200  $\mu$ m (D to F), and 100  $\mu$ m (G and H).



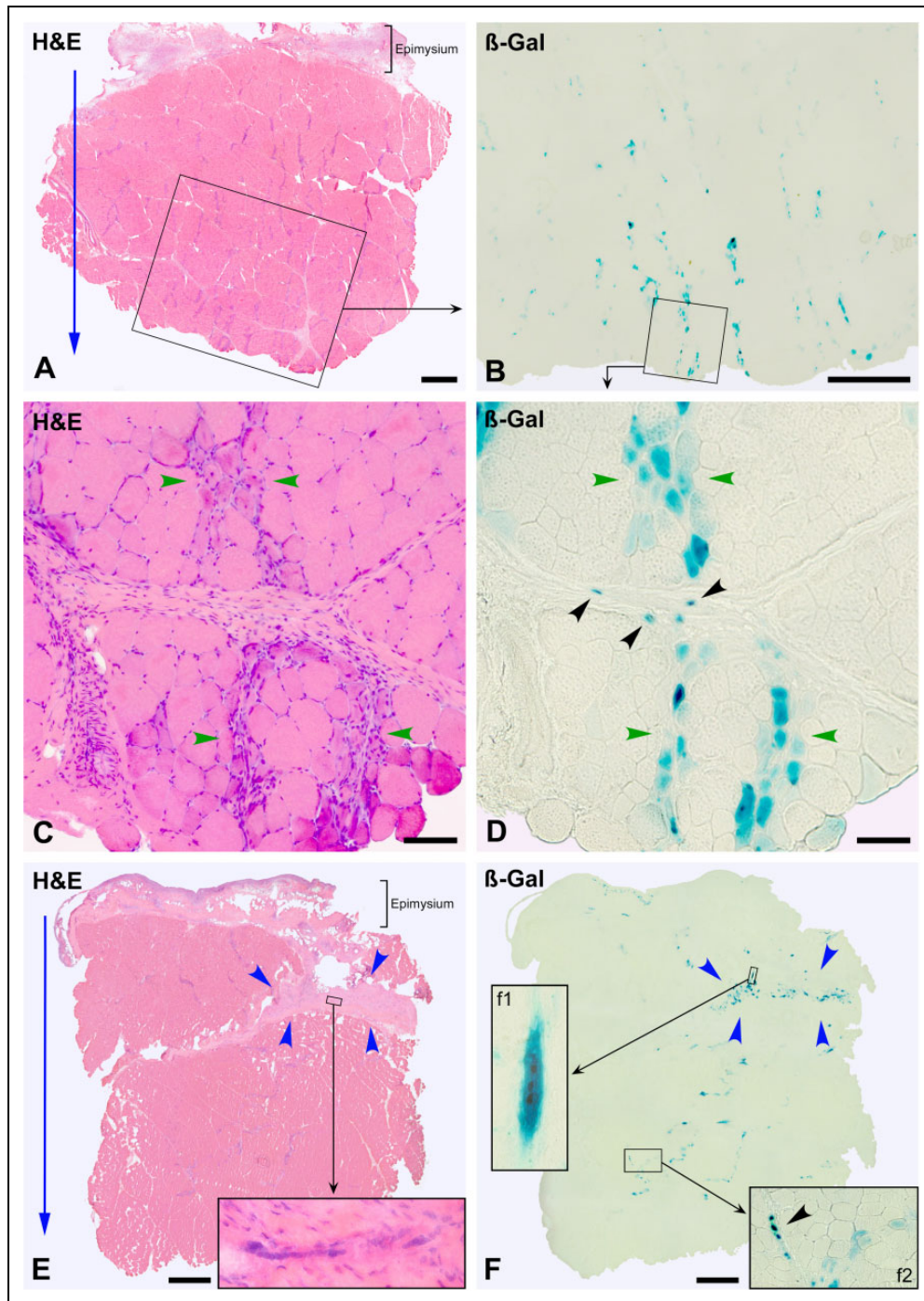


**Figure 5.** Muscle biopsies at post-cell transplantation (CT) day 7, stained with hematoxylin and eosin (H&E) and for  $\beta$ -Gal detection. A (monkey #6, biceps brachium) and E (monkey #5, quadriceps femoris) are whole cross sections with the outer surface upward. The cell injections followed the orientation of the blue arrows. Besides basophilic stripes formed by regenerating myofibers and thickening of the epimysium, no other alteration is visible. There are no clusters of mononuclear cells. (B) A serial section of the region in the rectangle in (A), where more  $\beta$ -Gal was observed. Most  $\beta$ -Gal is in the bands of regenerating myofibers (between green arrowheads in [C] and [D], an enlargement of the square in [B]).  $\beta$ -Gal is scarce but prefigures the pattern of bands of engraftment visible at post-CT wk 3. There are some small  $\beta$ -Gal+ elements in the perimysium (black arrowheads). (E) and (F) are serial sections, also showing scarce  $\beta$ -Gal detection. There is a large region of connective tissue (between blue arrowheads, probably corresponding to the connective tissue separating different portions of the quadriceps), which contains  $\beta$ -Gal+ elements, some of which are multinucleated myotubes (inset in [E] and inset f1 in [F]). Inset f2 (F) shows a region with  $\beta$ -Gal+ regenerating myofibers and some small  $\beta$ -Gal+ elements in the perimysium (arrowhead). Scale bars = 1 mm (A, B, E, and F) and 100  $\mu$ m (C, D).

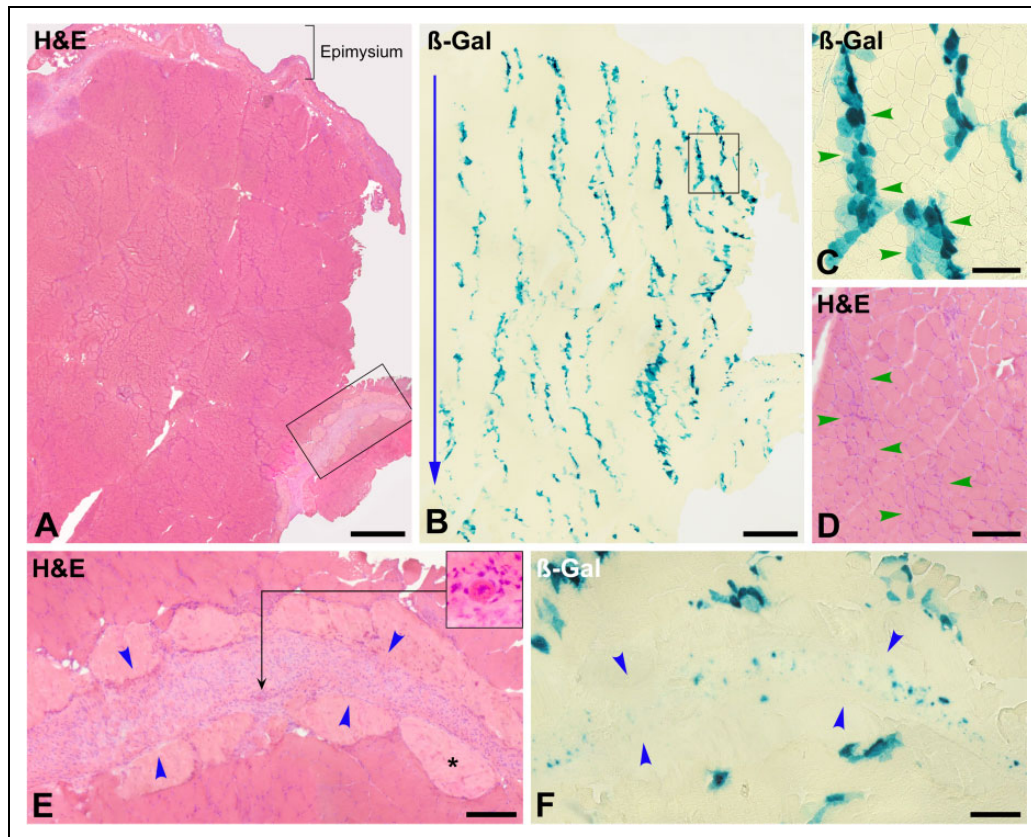


**Figure 6.** Muscle biopsy 3 wk post-cell transplantation (CT; monkey #5, quadriceps femoris). (A) and (B) are serial cross sections stained with hematoxylin and eosin (H&E) and for  $\beta$ -Gal detection. The outer muscle surface is upward, and the blue arrow indicates the orientation of the cell injections. Muscle histology is essentially normal, with the exception of myofibers with internal nuclei, some basophilia, and reduced size (D, between green arrowheads). The large majority of  $\beta$ -Gal is in myofibers, forming irregular and roughly parallel bands that coincide with the cell injection pattern (B). The region in the square in (B) is shown at higher magnification (C) with the corresponding serial H&E-stained section (D) to illustrate that  $\beta$ -Gal<sup>+</sup> myofibers in these bands (between green arrowheads) correspond to intrafascicular myofibers. There is a layer of connective tissue in (A), partially circumscribed by a rectangle that is shown at higher magnification in (E). It has a peripheral region of dense regular connective tissue with predominance of matrix (asterisk) and a central region with high cellularity (between blue arrowheads). The serial  $\beta$ -Gal-stained section (F) shows that this central region contains small  $\beta$ -Gal<sup>+</sup> elements. The inset in (E) shows the cross section of a myotube in this region. Scale bars = 1 mm (A and B) and 200  $\mu$ m (C to F).

of karyolysis at post-CT day 1), we sought to detect the main mechanisms of cell death, that is, necrosis and apoptosis. Intracellular MAC was observed in the accumulations of grafted cells at day 1 (Fig. 3E and H), evidencing significant grafted-cell necrosis at that time. MAC was not observed in the grafted cells at 1 h post-CT and was not frequent at d 3. Active caspase-3 was detected in the perimysial accumulations of grafted cells, mostly at day 1 (Fig. 3J and K). Nearly all cells that were active caspase-3<sup>+</sup> were negative for desmin (Fig. 3J and K). There were scarce active caspase-3<sup>+</sup> cells in the accumulations of grafted mononuclear cells at 1 h and day 3.

We also wanted to have an indication of whether the grafted cells proliferated, and for this purpose we immunodetected PCNA in the muscle sections (Fig. 8). However, since we failed to obtain an appropriate  $\beta$ -Gal immunodetection with the antibodies we tested, we were not able to co-detect PCNA specifically in the grafted cells, and therefore the interpretation of the results is limited in some periods.

Many nuclei were PCNA<sup>+</sup> 1 h after CT in the accumulations of grafted cells, with varying degrees of intensity (Fig. 8). PCNA<sup>+</sup> nuclei were also observed in the accumulations of grafted cells at post-CT day 1, although less abundant than 1 h after CT (Fig. 8). There were also PCNA<sup>+</sup> cells at post-CT day 3 in the grafted regions, but since  $\beta$ -Gal<sup>+</sup> cells were more dispersed and mixed with myofibers invaded by macrophages (as described above), which would be initiating the process of regeneration by activation of satellite cells and proliferation of the host's myoblasts, it was difficult to get an idea of whether PCNA was in grafted cells or recipient's cells at that time.

### Other General Observations

We did not observe blood collections in the biopsies at any time. This suggests that the vascular damage of the 27G needles used for injection was quite limited, and hemostasis was adequate.

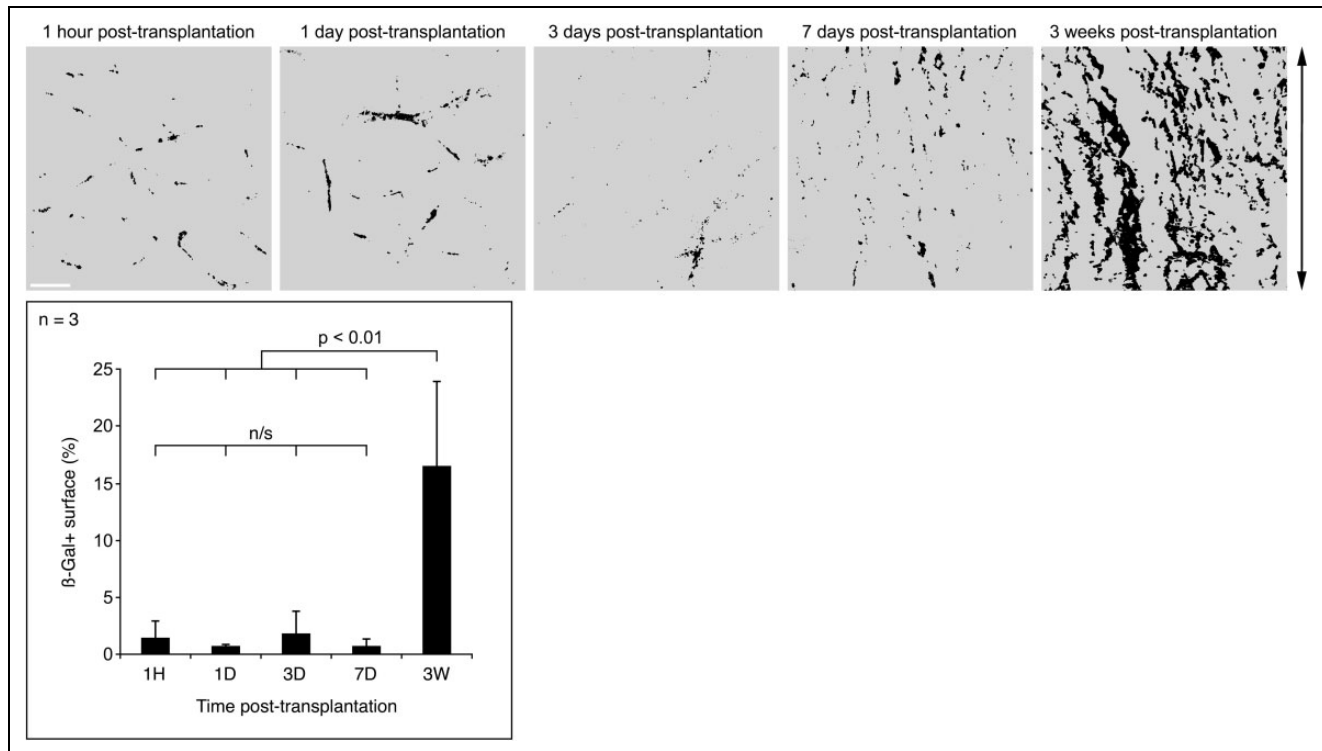


**Figure 7.** Changes in  $\beta$ -Gal distribution during the study. The top row shows the examples of  $\beta$ -Gal distribution in muscle sections at the periods studied (monkey #6).  $\beta$ -Gal is depicted in black and muscle in gray. Panels are at the same magnification (white scale bar = 1 mm). The arrow on the right indicates the course of the cell injections.  $\beta$ -Gal distribution was random at 1 h, days 1 and 3. At day 7,  $\beta$ -Gal is scarce but begins to orientate following the direction of injections. At 3 wk,  $\beta$ -Gal distribution constantly reproduces the injection pattern. The graph represents the area of the biopsy sections occupied by  $\beta$ -Gal in monkeys #5 to #7. This area increased dramatically at 3 wk post-cell transplantation (CT). n/s, nonsignificant; H, hour; D, day/s; W, weeks.

## Discussion

### Primary Grafted-Cell Distribution Versus Final CT Result

When we focused several years ago on defining CT techniques adapted to the large muscles of primates, we considered that we needed to distribute the cells as homogeneously as possible throughout the muscle.<sup>29</sup> For this purpose, we used matrices of parallel and equidistant injections, delivering small volumes of cell suspension along each injection trajectory.<sup>29,30</sup> One month after CT, muscle cross sections showed that myofibers expressing donor-derived proteins formed irregular bands that reminded the intramuscular injection trajectories. We called them bands of engraftment.<sup>10</sup>

Since at that time it was believed that grafted SCDMs lacked the ability to migrate into the recipient muscle,<sup>31</sup> we assumed that these bands of engraftment were due to the fact that the injected cells remained along the injection trajectories and fused with the adjacent myofibers. However, the present study confirms previous indications<sup>32</sup> that, even if the cell suspension is delivered homogeneously along each needle trajectory, the vast majority of the injected cells do not remain along those trajectories but are distributed

randomly in the perimysium. We were first surprised by the contrast between the very variable and erratic distribution of the grafted cells after injection and the constant long-term results of SCDM transplantation,<sup>21,30,33,34</sup> implying a rather homogeneous distribution of the hybrid myofibers throughout the muscle cross sections forming bands of engraftment with more or less overlap between them. Our interpretation of this discordance, now, is as follows:

- (a) The primary distribution of the injected cells is due to physical reasons (Fig. 9). CT implies the injection of a suspension (cells in saline) into a tissue in which different components (myofibers and connective tissue) may offer different resistance. The injected liquid will be submitted to compressive stress and pushed to flow into compliant regions (Fig. 9B). The perimysium appears to be less resistant than the endomysium to the penetration of the injected liquid, and easier to be split by this. Compression is potentially greater within the muscle bundles (perhaps due to the contractile tension of the myofibrils), tending to expel the injected suspension. The saline solution will be rapidly absorbed into the circulation, as any aqueous solution injected into the

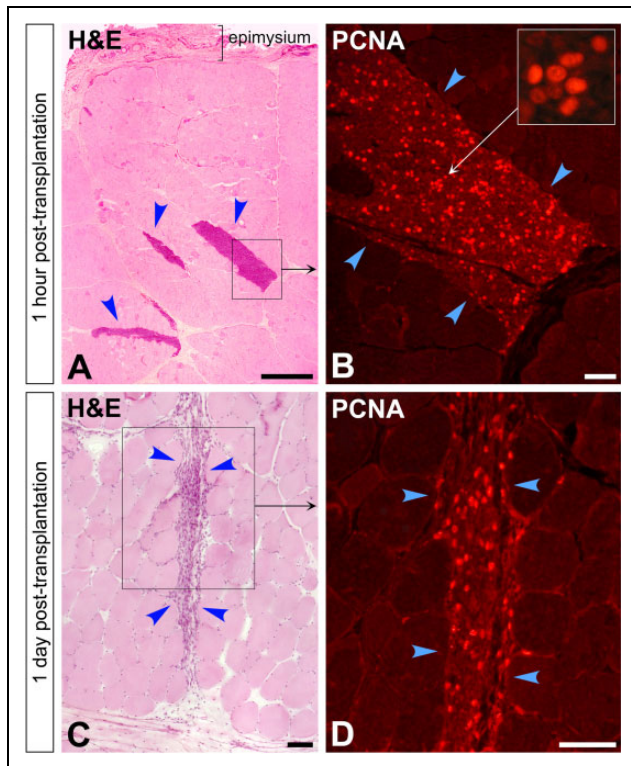


**Figure 8.** Cell proliferation in the intramuscular accumulations of grafted cells (arrowheads) evidenced by immunodetection of proliferating cell nuclear antigen (PCNA) in cross sections of muscle biopsies sampled at 1 h (A and B) and 1 d post-cell transplantation (CT; C and D). Again, the accumulations of grafted cells are seen as clusters of mononuclear cells in hematoxylin and eosin (H&E)-stained sections, more densely packed at 1 h (A) than at 1 d post-CT (C). The regions in the squares are shown at higher magnification in serial sections stained for fluorescent PCNA immunodetection. The inset in (B) shows some nuclei with different intensity of PCNA at higher magnification. Scale bars = 1 mm (A) and 100  $\mu$ m (B to D).

muscle,<sup>35</sup> and the grafted cells will become compacted (Fig. 9C). Some injected cells will remain in the intrafascicular injection trajectories probably because the needle damage severs myofibrils and causes a local loss of compression (Fig. 9C).

- (b) The graft outcome 3 wk later, on the other hand, reflects a biological phenomenon: the majority recruitment of the grafted SCDMs into the regeneration process of myofibers, which in the study conditions occurred almost exclusively in the myofibers damaged by the injections (see below).

### Observations on the Survival of Grafted Cells

In the accumulations of grafted cells, different phenomena occur (Fig. 10A and B). Some grafted cells die, clearly by necrosis and likely also by apoptosis. Necrosis is characterized by plasmalemma permeation leading to the intracellular

influx of extracellular molecules, including complement proteins. The complement is activated after intracellular penetration,<sup>36</sup> thus MAC is assembled and binds to intracellular elements.<sup>37</sup> Since the quaternary configuration of MAC has neoantigens not present in precursor molecules (such as C5b-9), the absence of native complement immunolabeling facilitates the demonstration of MAC deposition. This makes the intracellular MAC detection a reliable marker of necrosis.<sup>37</sup> On the other hand, we immunodetected the active form of caspase-3, which is useful to evidence apoptosis.<sup>38</sup> The presence of several elements that were active caspase-3 at post-CT day 1 suggests that some grafted cells developed a process of apoptosis early after CT. The fact that these elements are negative for desmin can be due to the degradation of this protein during apoptosis, since desmin is a substrate of caspases.<sup>39</sup> Necrosis and apoptosis were evident at post-CT day 1. Rare active caspase 3+ cells and no MAC+ cells were observed 1 h post-CT, even if some grafted cells were necrotic at the moment of CT as determined by the trypan blue exclusion test (average =  $6.4\% \pm 2.9\%$ ). This indicates that this period is too early to detect intracellular MAC deposition, as was also the case for damaged myofibers. Otherwise, the massive invasion by macrophages on day 3 implies that dead cells can rapidly undergo phagocytosis. It is therefore difficult to say whether the rare detection of caspase 3 active+ and MAC+ cells at post-CT day 3 is due to the fact that cell death no longer occurs or that dead cells are rapidly eliminated by phagocytosis. A recent study in monkeys, in fact, suggested that grafted SCDMs continue to die after post-CT day 3, but not after post-CT day 7.<sup>40</sup>

PCNA immunodetection identifies nuclei in the G1 and S phase and is useful to detect mitosis in tissue preparations.<sup>41,42</sup> In our study, PCNA detection suggests that some grafted cells proliferate after transplantation. However, since it was not possible for us to co-detect PCNA in the grafted cells (we failed to obtain an adequate  $\beta$ -Gal immunodetection as said above), it is not possible to say to what extent the PCNA detection indicates proliferation of the grafted cells in some periods. Since at 1 h post-CT is clear that the vast majority of the intramuscular mononuclear cell accumulations correspond to grafted cells (except for some inflammatory cells, which are postmitotic), we can affirm that PCNA detection in these accumulations indicates proliferation of grafted cells. PCNA+ nuclei among the grafted cells at 1 h are explained by the fact that the cells were grafted shortly after being harvested from proliferating cultures. At post-CT day 1, the grafted cell pockets are still well defined and seem to only be infiltrated by inflammatory cells so it is almost certain that PCNA detection also indicates proliferation of the grafted cells. At post-CT day 3, as explained above, the histological correlation was not clear, and we could not identify whether PCNA was in grafted or recipient's cells. Specific studies will be needed to evaluate during which time and to what extent the grafted SCDMs proliferate.

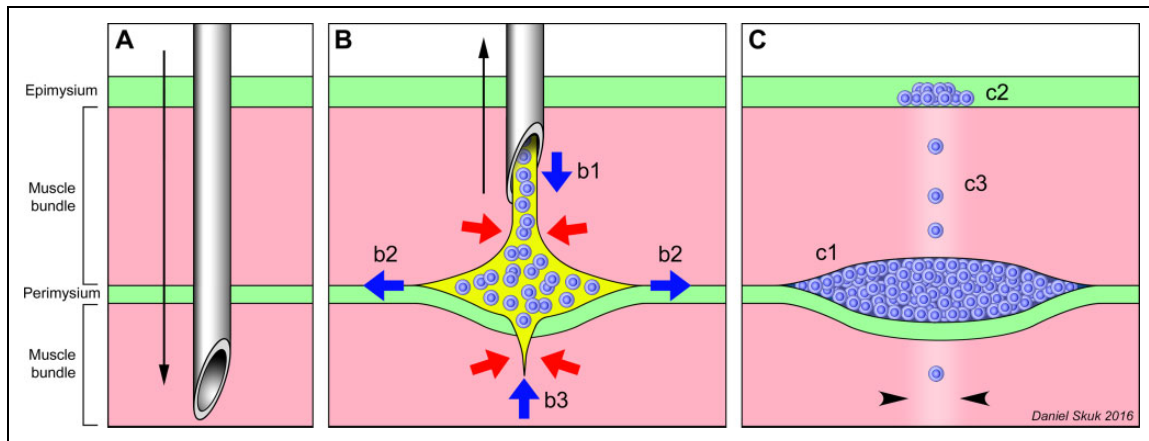


**Figure 9.** Interpretation of the early location of the injected cells. (A) Penetration (black arrow) of the injection needle through the muscle bundles (pink) and connective tissue (green). (B) Delivery of the cell suspension (blue = grafted cells, yellow = saline) during the needle withdrawal. Red arrows represent the compression exerted by the tissue on the cell suspension, and blue arrows represent the cell suspension displacements into the muscle. Even if the cell suspension is homogeneously delivered (b1) during the removal (black arrow) of the needle, it does not remain in the needle's trajectory but rather split the boundary between the perimysium and the muscle bundle (b2). The cell suspension may be expelled from the muscle bundles traversed by the needle (b3). (C) The final result, after saline absorption, is that most grafted cells are compacted in the periphery of muscle bundles (c1), some in the epimysium (c2), and only a few remain in the needle trajectory inside the fascicles (c3; the damage of the needle is represented by paler color, between arrowheads).

### Formation of Hybrid Myofibers Versus New Small Myofibers

Hybrid myofibers are formed by the fusion of the grafted MPCs with the recipient's myofibers. Since the recipient's myofibers are organized in muscle bundles, hybrid myofibers will be part of these bundles and, if regeneration is normal, will have a size similar to nonhybrid myofibers. This allows for the identification of hybrid myofibers, also with the fact that the expression of the graft-derived proteins occurs in a limited length, which can be seen following the myofibers in serial sections.

We can assume that the few grafted SCDMs remaining in the intrafascicular needle trajectories (if they survive, which was difficult to evaluate in our case) would participate in the regeneration of the nearby myofibers and would produce at least some hybrid myofibers. However, we demonstrated in monkeys that SCDMs grafted subcutaneously close to the outer muscle surface can migrate several millimeters to form hybrid myofibers after needle damage.<sup>32</sup> This indicates that hybrid myofibers can be largely produced by SCDMs that migrated from the extrafascicular cell accumulations (Fig. 10A and B). This seems to be supported by the fact that there was more  $\beta$ -Gal in the injection trajectories at day 3 than in the previous periods. Considering the intense macrophage infiltration in necrotic myofibers at day 3 and given that macrophages are the main source of chemotactic factors to SCDMs,<sup>43,44</sup> conditions exist for the grafted SCDMs to be recruited by myofiber regeneration during this post-CT period (Fig. 10A and B).

Otherwise, it seems clear that the small  $\beta$ -Gal+ elements in the perimysium at 3 wk post-CT are the remnants of the extrafascicular accumulations of  $\beta$ -Gal+ SCDMs produced

after the injection (Fig. 10B). The neoformation of myotubes and small myofibers may take place by the grafted SCDMs that survive in the extrafascicular accumulations, that do not migrate, and that fuse with their neighboring counterparts.

For the moment, it may only be speculated why there was a striking increase in the  $\beta$ -Gal+ surface at 3 wk post-CT.  $\beta$ -Gal expression in the grafted cells is strong immediately after CT, and the  $\beta$ -Gal+ surface observed 1 h post-CT is only dependent on the number of cells in the muscle cross section. It is possible that the largest  $\beta$ -Gal+ surface observed at 3 wk is due to the fact that  $\beta$ -Gal diffuses and accumulates in a larger cytoplasm, given the large amount of sarcoplasm that contains a myofiber in relation to the myonuclei and the greater cross-sectional area of myofibers with respect to mononuclear cells. However, at post-CT day 7, most grafted cells appear to have already fused with the recipient's myofibers, but the expression of  $\beta$ -Gal in these regenerating myofibers is much weaker and more dispersed than in the mature myofibers at post-CT wk 3. We can assume that once the regeneration process is over, the  $\beta$ -Gal promoter activity is stronger or that more graft-derived myonuclei are active than during regeneration, together with a greater accumulation of  $\beta$ -Gal in the sarcoplasm once the myofiber is mature and stable. In fact, it has been reported that not all myonuclei are active during myofiber regeneration.<sup>45</sup>

### How These Findings Meet Clinical Observations?

The present study provides insight into some observations we made in a clinical trial of SCDM transplantation in DMD patients.<sup>5</sup> The analysis of muscle biopsies at that time made us differentiate 2 types of myofibers expressing donor-

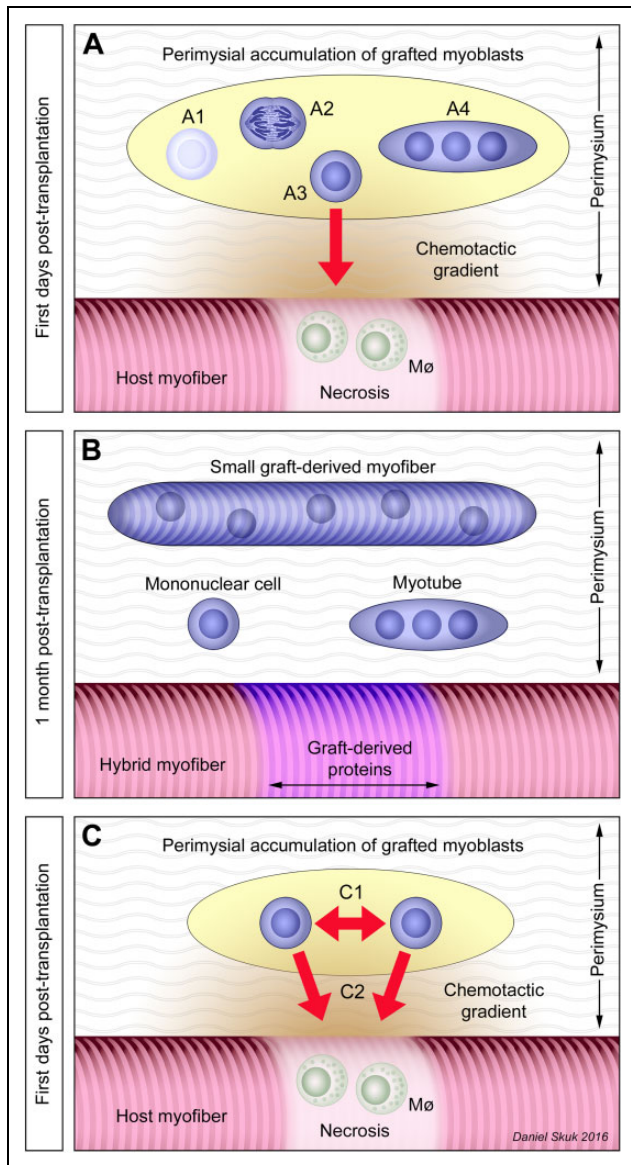


**Figure 10.** Interpretation of the graft evolution. Graft-derived elements are represented in blue. (A) Grafted satellite cell-derived myoblasts (SCDMs) that accumulated in the perimysium may have different fates. Some die (A1) by necrosis or apoptosis, while at least some survivors may proliferate (A2). Some grafted SCDMs may migrate (A3) attracted by chemotactic gradients (represented in orange) toward damaged myofibers in which there is segmental necrosis with macrophage (M $\phi$ ) recruitment that launched a process of regeneration. Finally, some grafted SCDMs fuse with each other (A4) in their original location, forming myotubes and eventually small myofibers. (B) After 3 wk, the process is completed: the compact accumulations of grafted cells have disappeared leading some isolated graft-derived elements in the perimysium: mononuclear cells, myotubes, and small myofibers. On the other hand, hybrid myofibers in the muscle bundles are the result of the fusion of grafted SCDMs with the recipient's myofibers. (C) Grafted SCDMs in the extrafascicular accumulations would be subject to 2 opposing forces: a tendency to fuse with neighboring grafted SCDMs (C1) and the attraction of chemotactic gradients to migrate toward regenerating myofibers (C2).

derived dystrophin (Fig. 11). One type (referred to as “A”) corresponded to dystrophin+ myofibers integrated into the muscle bundles and similar in size to the dystrophin-negative myofibers. When we analyzed these myofibers through several serial sections, we observed that the expression of donor-derived dystrophin was restricted to a few millimeters.<sup>6</sup> These myofibers were therefore hybrid, which means that the expression of dystrophin was due to genetic complementation after the fusion of the grafted SCDMs with the host myofibers. They were roughly disposed in irregular bands corresponding to the cell-injection trajectories. The other type of donor-derived myofibers (referred to as “B”) was represented by short and small myofibers scattered throughout focal accumulations of connective tissue (Fig. 11). Since these small myofibers were short and entirely donor-dystrophin+, we interpreted that they corresponded to myofiber neof ormation due to fusion of the grafted SCDMs with each other.

We can now interpret that in these DMD patients transplanted with normal SCDMs, there was a phenomenon similar to that described in the present study. The injected SCDMs formed extrafascicular accumulations where they fused with each other to produce the type B myofibers. On the other hand, both the few grafted SCDMs that potentially remained in the injection trajectories as well as the SCDMs that might have migrated from the extrafascicular accumulations, generated the type A myofibers, that is, hybrid myofibers.

### How Can These Observations Be Useful?

It is plausible to conceive that the grafted MPCs that survive in the extrafascicular accumulations will be subject to 2 opposing forces (Fig. 10C). On the one hand, chemotactic gradients will stimulate them to migrate toward damaged myofibers to participate in myofiber regeneration and, on the other hand, they will tend to fuse with the neighboring grafted MPCs to form new myotubes. The predominance of one force over the other will condition the result of the graft. Macrophages are the main source of chemotactic substances for SCDMs<sup>43,44</sup> and in this study, there were large amounts of macrophages concentrated in the damaged myofibers. Therefore, chemotactic migration toward damaged myofibers is likely to be the predominant force in the study conditions.

From the point of view of CT, this could imply that:

- If our priority is to produce hybrid myofibers to obtain therapeutic levels of genetic complementation, primacy should be given to producing sufficient myofiber regeneration concomitant to CT<sup>24,46</sup> and, if possible, increase the diffusion ability of grafted MPCs during this process.
- If our priority is to produce new myofibers, we should produce extrafascicular cell accumulations infiltrating the tissue for long distances, reducing

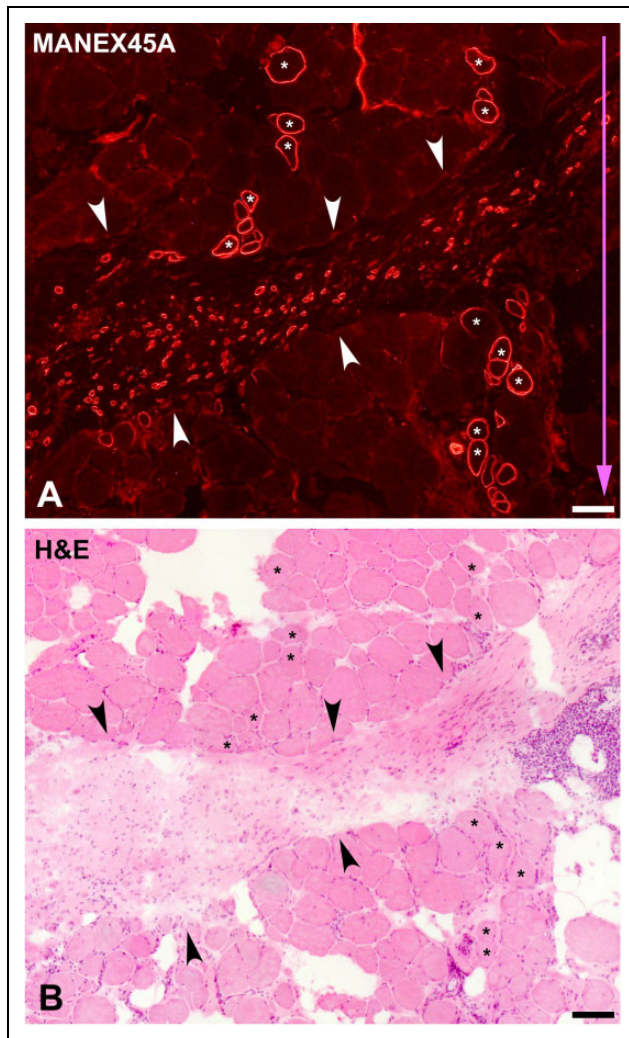


**Figure 11.** Serial cross sections of a muscle biopsy in a cell-grafted region (patient #1) of our last clinical trial of satellite cell-derived myoblast (SCDM) transplantation in Duchenne muscular dystrophy (DMD) patients.<sup>5</sup> SCDMs were implanted by 25 parallel injections in 1 cm<sup>3</sup> of muscle and delivered in each needle trajectory. Sections were stained for immunodetection of dystrophin with the MANEX45A monoclonal antibody (A) and with hematoxylin and eosin (H&E) (B). H&E shows features of DMD: increased connective tissue, adipocyte infiltration, and myofibers of rounded profiles and variable sizes with internal myonuclei and splitting. MANEX45A detects an epitope coded by exon 45, and DMD in this patient was caused by a deletion of exon 45, thus dystrophin in A is from donor origin. As explained in the text, there are 2 types of dystrophin+ myofibers in this biopsy. One corresponds to myofibers into the muscle bundles (some indicated with asterisks) of similar sizes as the dystrophin-negative myofibers. They were hybrid myofibers, that is, dystrophin production was due to the fusion of the grafted SCDMs with the recipient's myofibers. They form tracks corresponding to the injection trajectories, whose direction is indicated by the blue arrow. The other myofiber type is represented by short and small-sized myofibers dispersed in an accumulation of connective tissue (between arrowheads). The present study supports and explains our previous interpretation that these myofibers were neofomed by the fusion of the grafted SCDMs with each other. Scale bars = 100  $\mu$ m.

myofiber damage to the minimum to reduce the myofiber regeneration necessary to attract the grafted MPCs. This should be complemented with strategies to improve the survival of the grafted cells and to promote the fusion with each other in a complete and organized manner, parallel to the myofibers of the host muscle. The use of scaffolds<sup>47,48</sup> or extracellular matrix components<sup>47,49,50,51</sup> for CT must thus be tested in monkeys in this context. However, to form these cell accumulations, we must keep in mind that we are limited by the fact that oxygen does not diffuse enough to prevent ischemia death beyond a diameter of 200 to 400  $\mu$ m.<sup>25</sup>

Indeed, the present observations apply to CT in a muscle whose structure is preserved. It remains to be studied what occurs in muscles that have partially or totally degenerated with loss of myofibers and replacement by fibrous and/or adipose tissue.

### Authors' Note

D.S. contributed to conceptualization, methodology, validation, formal analysis, investigation, visualization, project administration and writing. D.S. and J.P.T. contributed to review and funding acquisition and resources.

### Acknowledgments

The authors wish to express their gratitude to Ms Marlyne Goulet and Mr Martin Paradis for their excellent technical work and to Steve Brochu for his technical assistance during monkey procedures.

### Ethical Approval

This study was approved by the Laval University Animal Care Committee (CPAUL).

### Statement of Human and Animal Rights

We declare that the experiments on nonhuman primates were conducted in accordance with local Ethical Committee laws and regulations as regards care and use of laboratory animals.

### Statement of Informed Consent

There are no human subjects in this article. Therefore, informed consent is not applicable.

### Declaration of Conflicting Interests

The author(s) declared no potential conflicts of interest with respect to the research, authorship, and/or publication of this article.

### Funding

The author(s) disclosed receipt of the following financial support for the research and/or authorship of this article: This work was supported by a grant of the Jesse's Journey Foundation for Gene and Cell Therapy of Canada to D.S. and a grant of the Canadian Institutes of Health Research to J.P.T.

## References

- Skuk D, Tremblay JP. Cell therapy in muscular dystrophies: many promises in mice and dogs, few facts in patients. *Expert Opin Biol Ther.* 2015.
- Carlson BM, Gutmann E. Regeneration in free grafts of normal and denervated muscles in the rat: morphology and histochemistry. *Anat Rec.* 1975;183(1):47–62.
- Vilquin JT, Catelain C, Vauchez K. Cell therapy for muscular dystrophies: advances and challenges. *Curr Opin Organ Transplant.* 2011;16(6):640–649.
- Mendell JR, Kissel JT, Amato AA, King W, Signore L, Prior TW, Sahenk Z, Benson S, McAndrew PE, Rice R, et al. Myoblast transfer in the treatment of Duchenne's muscular dystrophy. *N Engl J Med.* 1995;333(13):832–838.
- Skuk D, Goulet M, Roy B, Chapdelaine P, Bouchard JP, Roy R, Dugre FJ, Sylvain M, Lachance JG, Deschenes L, et al. Dystrophin expression in muscles of Duchenne muscular dystrophy patients after high-density injections of normal myogenic cells. *J Neuropathol Exp Neurol.* 2006;65(4):371–386.
- Skuk D, Goulet M, Roy B, Piette V, Cote CH, Chapdelaine P, Hogrel JY, Paradis M, Bouchard JP, Sylvain M, et al. First test of a "high-density injection" protocol for myogenic cell transplantation throughout large volumes of muscles in a Duchenne muscular dystrophy patient: eighteen months follow-up. *Neuromuscul Disord.* 2007;17(1):38–46.
- Skuk D, Paradis M, Goulet M, Chapdelaine P, Rothstein DM, Tremblay JP. Intramuscular transplantation of human postnatal myoblasts generates functional donor-derived satellite cells. *Mol Ther.* 2010;18(9):1689–1697.
- Skuk D, Roy B, Goulet M, Chapdelaine P, Bouchard JP, Roy R, Dugre FJ, Lachance JG, Deschenes L, Helene S, et al. Dystrophin expression in myofibers of Duchenne muscular dystrophy patients following intramuscular injections of normal myogenic cells. *Mol Ther.* 2004;9(3):475–482.
- Skuk D, Tremblay JP. Confirmation of donor-derived dystrophin in a Duchenne muscular dystrophy patient allotransplanted with normal myoblasts. *Muscle Nerve.* 2016;54(5):979–981.
- Skuk D. Cell transplantation and "stem cell therapy" in the treatment of myopathies: many promises in mice, few realities in humans. *ISRN Stem Cells.* 2013;(2013):25. Article ID 582689.
- Hagege AA, Carrion C, Menasche P, Vilquin JT, Duboc D, Marolleau JP, Desnos M, Bruneval P. Viability and differentiation of autologous skeletal myoblast grafts in ischaemic cardiomyopathy. *Lancet.* 2003;361(9356):491–492.
- Skuk D. Myoblast transplantation for inherited myopathies: a clinical approach. *Expert Opin Biol Ther.* 2004;4(12):1871–1885.
- Perie S, Trollet C, Mouly V, Vanneaux V, Mamchaoui K, Bouazza B, Marolleau JP, Laforet P, Chapon F, Eymard B, et al. Autologous myoblast transplantation for oculopharyngeal muscular dystrophy: a phase I/IIa clinical study. *Mol Ther.* 2014;22(1):219–225.
- Vilquin JT, Marolleau JP, Sacconi S, Garcin I, Lacassagne MN, Robert I, Ternaux B, Bouazza B, Larghero J, Desnuelle C. Normal growth and regenerating ability of myoblasts from unaffected muscles of facioscapulohumeral muscular dystrophy patients. *Gene Ther.* 2005;12(22):1651–1662.
- Peters KM, Dmochowski RR, Carr LK, Robert M, Kaufman MR, Siris LT, Herschorn S, Birch C, Kultgen PL, Chancellor MB. Autologous muscle derived cells for treatment of stress urinary incontinence in women. *J Urol.* 2014;192(2):469–476.
- Frudinger A, Kolle D, Schwaiger W, Pfeifer J, Paede J, Halligan S. Muscle-derived cell injection to treat anal incontinence due to obstetric trauma: pilot study with 1 year follow-up. *Gut.* 2010;59(1):55–61.
- Anderson DJ, Kirk AD. Primate models in organ transplantation. *Cold Spring Harb Perspect Med.* 2013;3(9):a015503.
- Skuk D, Goulet M, Paradis M, Tremblay JP. Myoblast transplantation: techniques in nonhuman primates as a bridge to clinical trials. In: Soto-Gutierrez A, Navarro-Alvarez N, Fox IJ, editors. *Methods in bioengineering: cell transplantation.* Boston (MA): Artech House; 2011:219–236.
- Skuk D, Tremblay JP. Intramuscular cell transplantation as a potential treatment of myopathies: clinical and preclinical relevant data. *Expert Opin Biol Ther.* 2011;11(3):359–374.
- Ham RG, St. Clair JA, Webster C, Blau HM. Improved media for normal human muscle satellite cells: serum-free clonal growth and enhanced growth with low serum. *In Vitro Cell Dev Biol.* 1988;24(8):833–844.
- Skuk D, Goulet M, Tremblay JP. Intramuscular transplantation of myogenic cells in primates: importance of needle size, cell number, and injection volume. *Cell Transplant.* 2014;23(1):13–25.
- Skuk D, Caron NJ, Goulet M, Roy B, Espinosa F, Tremblay JP. Dynamics of the early immune cellular reactions after myogenic-cell transplantation. *Cell Transplant.* 2002;11(7):671–681.
- Skuk D, Caron NJ, Goulet M, Roy B, Tremblay JP. Resetting the problem of cell death following muscle-derived cell transplantation: detection, dynamics and mechanisms. *J Neuropathol Exp Neurol.* 2003;62(9):951–967.
- Skuk D, Goulet M, Tremblay JP. Electroporation as a method to induce myofiber regeneration and increase the engraftment of myogenic cells in skeletal muscles of primates. *J Neuropathol Exp Neurol.* 2013;72(8):723–734.
- Skuk D, Paradis M, Goulet M, Tremblay JP. Ischemic central necrosis in pockets of transplanted myoblasts in nonhuman primates: implications for cell-transplantation strategies. *Transplantation.* 2007;84(10):1307–1315.
- Stadelmann C, Lassmann H. Detection of apoptosis in tissue sections. *Cell Tissue Res.* 2000;301(1):19–31.
- Skuk D. Acute rejection of myofibers in nonhuman primates: key histopathologic features. *J Neuropathol Exp Neurol.* 2012;71(5):398–412.
- Dubowitz V, Sewry CA. *Muscle biopsy: a practical approach.* 3rd ed. Philadelphia (PA): Saunders/Elsevier; 2007.
- Skuk D, Goulet M, Roy B, Tremblay JP. Myoblast transplantation in whole muscle of nonhuman primates. *J Neuropathol Exp Neurol.* 2000;59(3):197–206.



30. Skuk D, Goulet M, Roy B, Tremblay JP. Efficacy of myoblast transplantation in nonhuman primates following simple intramuscular cell injections: toward defining strategies applicable to humans. *Exp Neurol*. 2002;175(1):112–126.
31. Skuk D, Tremblay JP. Clarifying misconceptions about myoblast transplantation in myology. *Mol Ther*. 2014;22(5):897–898.
32. Skuk D, Goulet M, Tremblay JP. Transplanted myoblasts can migrate several millimeters to fuse with damaged myofibers in nonhuman primate skeletal muscle. *J Neuropathol Exp Neurol*. 2011;70(9):770–778.
33. Quenneville SP, Chapdelaine P, Skuk D, Paradis M, Goulet M, Rousseau J, Xiao X, Garcia L, Tremblay JP. Autologous transplantation of muscle precursor cells modified with a lentivirus for muscular dystrophy: human cells and primate models. *Mol Ther*. 2007;15(2):431–438.
34. Skuk D, Goulet M, Tremblay JP. Use of repeating dispensers to increase the efficiency of the intramuscular myogenic cell injection procedure. *Cell Transplant*. 2006;15(7):659–663.
35. Shargel L, Wu-Pong S, Yu A. *Applied biopharmaceutics and pharmacokinetics*. 6th ed. New York (NY): McGraw-Hill Medical; 2012.
36. Engel AG, Biesecker G. Complement activation in muscle fiber necrosis: demonstration of the membrane attack complex of complement in necrotic fibers. *Ann Neurol*. 1982;12(3):289–296.
37. Thomsen H, Held H. Immunohistochemical detection of C5b-9(m) in myocardium: an aid in distinguishing infarction-induced ischemic heart muscle necrosis from other forms of lethal myocardial injury. *Forensic Sci Int*. 1995;71(2):87–95.
38. Mukasa T, Momoi T, Momoi MY. Activation of caspase-3 apoptotic pathways in skeletal muscle fibers in laminin alpha2-deficient mice. *Biochem Biophys Res Commun*. 1999;260(1):139–142.
39. Chen F, Chang R, Trivedi M, Capetanaki Y, Cryns VL. Caspase proteolysis of desmin produces a dominant-negative inhibitor of intermediate filaments and promotes apoptosis. *J Biol Chem*. 2003;278(9):6848–6853.
40. Skuk D, Tremblay JP. Cell therapy in myology: dynamics of muscle precursor cell death after intramuscular administration in non-human primates. *Mol Ther Methods Clin Dev*. 2017;5:232–240.
41. Bacchi CE, Gown AM. Detection of cell proliferation in tissue sections. *Braz J Med Biol Res*. 1993;26(7):677–687.
42. Mahler M, Miyachi K, Peebles C, Fritzler MJ. The clinical significance of autoantibodies to the proliferating cell nuclear antigen (PCNA). *Autoimmun Rev*. 2012;11(10):771–775.
43. Robertson TA, Maley MA, Grounds MD, Papadimitriou JM. The role of macrophages in skeletal muscle regeneration with particular reference to chemotaxis. *Exp Cell Res*. 1993;207(2):321–331.
44. Saclier M, Cuvellier S, Magnan M, Mounier R, Chazaud B. Monocyte/macrophage interactions with myogenic precursor cells during skeletal muscle regeneration. *FEBS J*. 2013;280(17):4118–4130.
45. Newlands S, Levitt LK, Robinson CS, Karpf AB, Hodgson VR, Wade RP, Hardeman EC. Transcription occurs in pulses in muscle fibers. *Genes Dev*. 1998;12(17):2748–2758.
46. Skuk D, Roy B, Goulet M, Tremblay JP. Successful myoblast transplantation in primates depends on appropriate cell delivery and induction of regeneration in the host muscle. *Exp Neurol*. 1999;155(1):22–30.
47. Borselli C, Cezar CA, Shvartsman D, Vandenberg HH, Mooney DJ. The role of multifunctional delivery scaffold in the ability of cultured myoblasts to promote muscle regeneration. *Biomaterials*. 2011;32(34):8905–8914.
48. Hill E, Boontheekul T, Mooney DJ. Designing scaffolds to enhance transplanted myoblast survival and migration. *Tissue Eng*. 2006;12(5):1295–1304.
49. Casar JC, Cabello-Verrugio C, Olguin H, Aldunate R, Inestrosa NC, Brandan E. Heparan sulfate proteoglycans are increased during skeletal muscle regeneration: requirement of syndecan-3 for successful fiber formation. *J Cell Sci*. 2004;117(pt 1):73–84.
50. Mikami T, Koyama S, Yabuta Y, Kitagawa H. Chondroitin sulfate is a crucial determinant for skeletal muscle development/regeneration and improvement of muscular dystrophies. *J Biol Chem*. 2012;287(46):38531–38542.
51. Silva-Barbosa SD, Butler-Browne GS, de Mello W, Riederer I, Di Santo JP, Savino W, Mouly V. Human myoblast engraftment is improved in laminin-enriched microenvironment. *Transplantation*. 2008;85(4):566–575.